X-ray tube focal spot assessment using pinhole digital radiography with a compact detector: Signal extraction and mechanical design

2026 JULY 19–22 VANCOUVER, BC
JOINT AAPM | COMP MEETING

Grant A. Budge,[1,*] Andre Ramos Moreno,[2] Paul C. Johns[1,**]

[1]Physics Dept., Carleton University, Ottawa, Canada,
[2]Div. Ciencias e Ingenierías, Univ. Guanajuato, León de Los Aldama, México

Carleton University

Ottawa Medical Physics Institute

PO-DPV-D-13

ABSTRACT

Purpose: The x-ray tube focal spot is a key determinant of imaging system resolution. Digital pinhole radiography yields the source point spread function (PSF_{source}) in addition to the nominal size. Using a compact digital detector of a type used in dentistry and noting the IEC Standard 60336:2020 pinhole radiography requirements, we investigate extraction of faint image patterns in the presence of x-ray statistics and detector noise, and design a robust and versatile mechanical system for source-pinhole-detector alignment.

Methods: A CsI(Tl)/CMOS 20-µm 1000 x 1500 element detector (Hamamatsu S11684-12) and pinholes of 75 and 30 µm (RaySafe) were used to evaluate a Picker Dunlee PX412A / DU304 x-ray tube, focal spot nominal values 0.6, 1.2, by summing multiple exposures acquired in detector manual mode. Fixed pattern noise from the row-sequential readout was minimized via normalization (Matlab). Several mechanical designs were considered for alignment plus measurement of enlargement factor (image size/source size) via a scale object when direct distance measurement is obstructed.

Results: The detector software's standard flat-field normalization was insufficient to remove background degradation of faint focal spot patterns. Normalizing the focal spot pattern, using regions external to the focal spot in the same image, provided better data. Most IEC requirements were met, but SNR > 100 was not. A camera structure has been designed but not yet fabricated. The design comprises stackable aluminum box frames of heights 10, 20, 40 cm, the combinations of which give pinhole-to-detector distances 10,20,30, ...,70 cm.

Conclusion: Digital focal spot pinhole radiography, employing multiple exposures and fixed pattern normalization using part of same image, gives directly PSF_{source}. Due to low focal spot image fluence the IEC requirement on SNR is difficult to meet, but in any case, measurement uncertainty can be propagated to the final nominal size. A versatile camera mechanical system has been designed.

CONTACTS

* GrantBudge@cmail.carleton.ca
** Paul.Johns@carleton.ca

Dept. Physics, Carleton University
1125 Colonel By Drive
Ottawa, ON K1S 5B6 Canada

INTRODUCTION

While IEC (Ref. 1) **specifies** that focal spots be assessed using **slit radiography + LSF, other methods are also permitted** (p. 23, sect. 9). The major benefit of pinhole radiography is that it directly gives PSF_{source}. We examine **digital pinhole radiography** in light of three IEC requirements (Ref. 1 p. 17, sect. 6.3.2):

(i) focal spot width ≥ 60 pixels at 15% max intensity,
(ii) max signal ≥ 200 levels above background region,
(iii) Signal-to-Noise Ratio (SNR) ≥ 100.

The **variables** across tests were: enlargement (E), pinhole size, exposure time, tube current.

$$E = \frac{d_{SR} - d_{SP}}{d_{SP}} \text{ with } d_{SR},\ d_{SP} \text{ as in Fig. 1.}$$

Pinhole imaging is **challenging due to image faintness.** Use of a **high-resolution detector** helps with criterion (i), while **reducing *E*** helps with (ii), (iii) provided that E is not so small that (i) is not met.

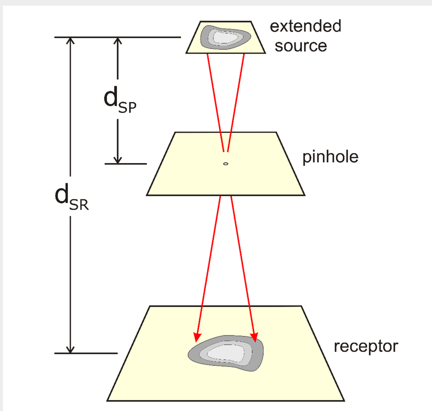

Fig. 1. Geometry.

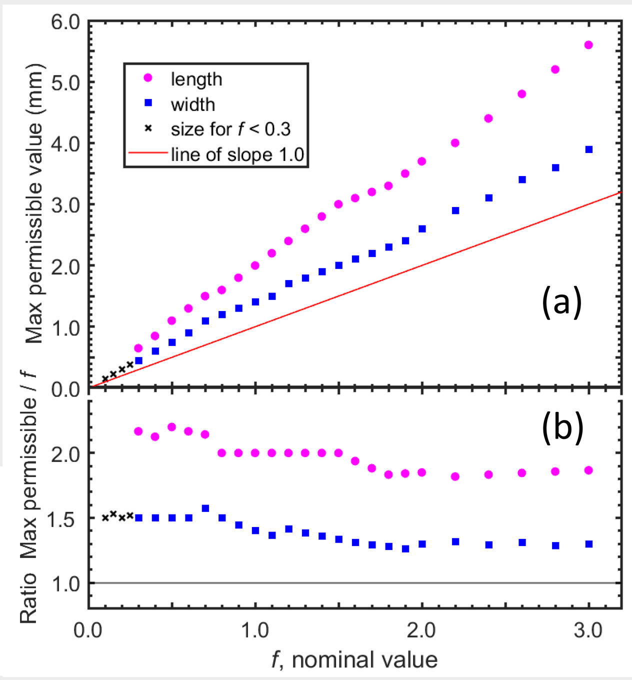

Fig. 2. (a) IEC 2020 Table 3 max allowed sizes (mm) vs nominal value f (unitless). (b) their ratio.

The IEC process results in a **dimensionless nominal value *f***, as given in Table 3 of IEC 2020, which is marked on serial plates. The **actual dimensions (mm) can be significantly larger than the value of *f*.** See Fig. 2.

METHODS AND MATERIALS

See Fig. 3. Our test source was a Picker Dunlee x-ray tube with nominal focal spot sizes 0.6, 1.2, driven by a single-phase generator. **In this poster, results for measurement of the 1.2 focal spot are shown as an example.**
A **Hamamatsu S11684-12 detector**, previously evaluated in our lab,[2] acquired the images. For **alignment**, a **metal tube**, machined with a perpendicular end, was placed directly on the detector which was then moved until the tube radiographed as a circle indicating that the detector was at the central axis and perpendicular to it. The cylinder was then removed and the pinhole positioned so that its image was where the cylinder's had been.

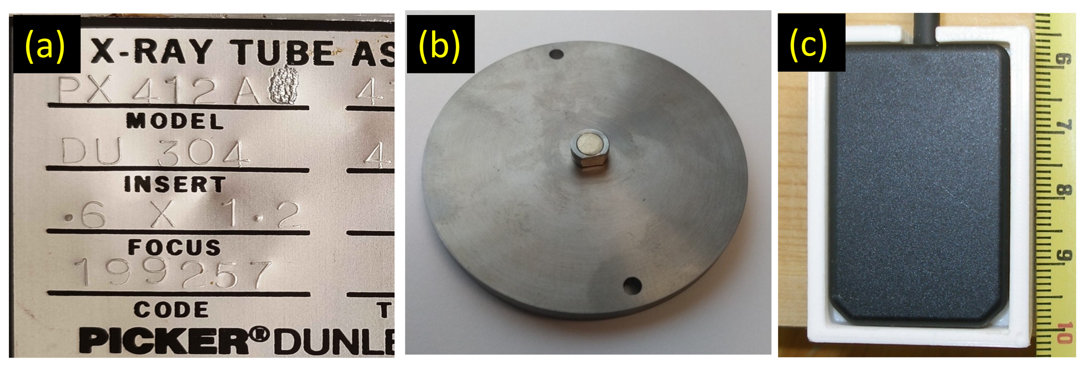

Fig. 3. (a) x-ray tube serial plate, f = 0.6, 1.2. (b) Raysafe 75 µm pinhole on W/Cu disk. (c) Hamamatsu S11684-12 sensor, CsI/CMOS, 20 µm elements, 1000x1500, in 3d-printed holder.

REFERENCES

1. IEC Std 60336 ed. 5.0, *Medical electrical equipment - X-ray tube assemblies for medical diagnosis – Focal spot dimensions and related characteristics* (Internat. Electrotechnical Commission, Geneva, Switzerland, 2020) + Corr. 1 (2022). (ISBN 978-2-8322-9162-7).
2. E.T.E. Anderson and P.C. Johns, COMP annual conf., abstract, Med. Phys. **49** (8), 5645-5645 (2022), doi: 10.1002/mp.15896.

RESULTS

We show **example results** for measurement of the 1.2 focal spot. Fig. 4(a) shows a **typical single acquisition**: 60 kV, 200 mA, 100 ms, 75 µm pinhole at d_{SP} = 387 mm, enlargement E = 0.760. The maximum focal spot data value is 5587, while the adjacent background's mean is 5336, a difference of 251, thus meeting requirement (ii).

In a single acquisition the focal spot is noticeably faint versus its surroundings and therefore to improve SNR, 10 focal spot acquisitions (**X**), 10 dark field (**D**), and 10 uniform field gain acquisitions (**G**) were obtained. Standard **flat field correction** (**FFC**) was performed in Matlab as $FFC = (X - D)\frac{\langle G-D \rangle}{G-D}$. Figs. 4(b),(c) show the result. Residual **row-to-row texture** remains due to the detector's row-sequential readout.
In Fig. 5 a **row-to-row correction** is applied using regions-of-interest (ROI) outside of the focal spot area.
The resulting image was then used to generate height and width **line spread functions (LSF)**. For this example, the width LSF (Fig. 6) has 15% size of 82 pixels or 1.64 mm. After correction for E and blurring, the **focal spot width** is 1.98 mm.

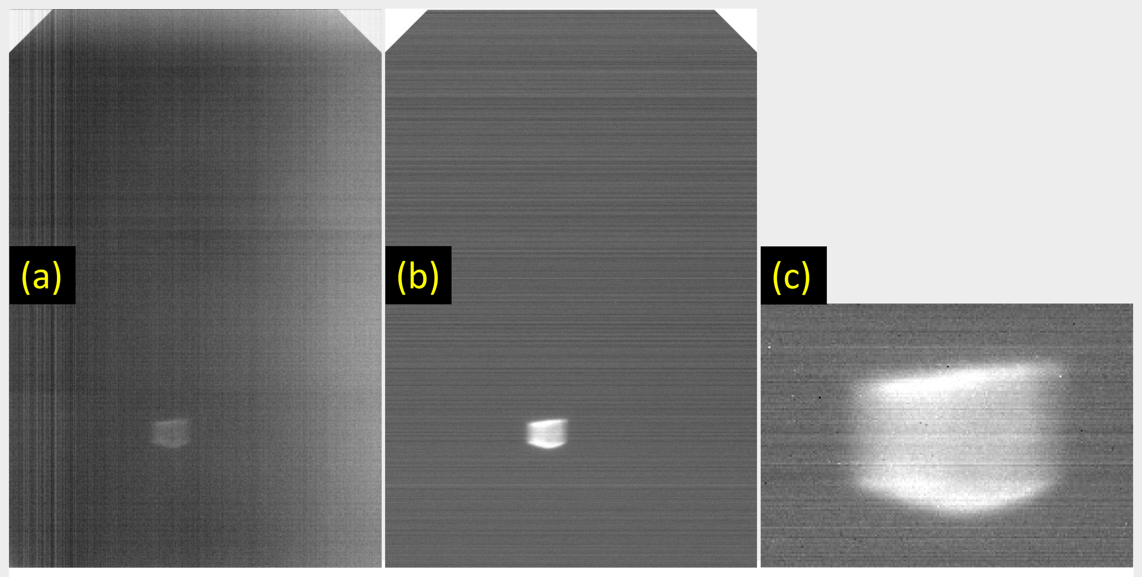

Fig. 4. (a) Single raw image, before dark correction. Display level = 5451, window = 492. (b) Result of FFC on average of 10 pinhole acquisitions, 10 dark, 10 gain. (c) Enlarged view, lev/win adjusted.

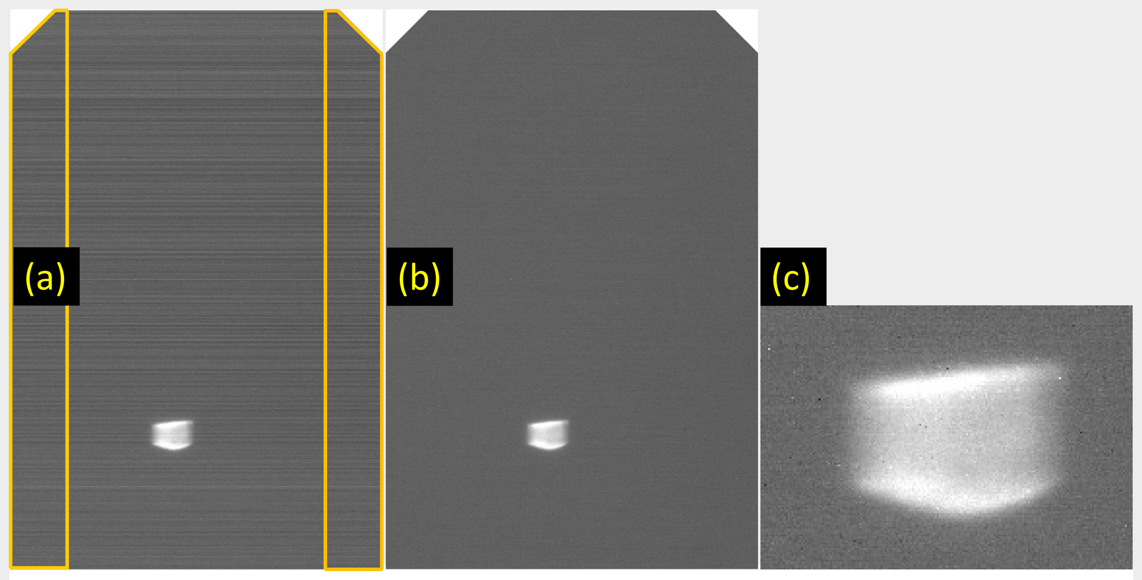

Fig. 5. (a) Two 150-column-wide regions used for row-to-row correction. (b) After row-to-row correction. (c) Enlarged view of final focal spot image, lev/win adjusted.

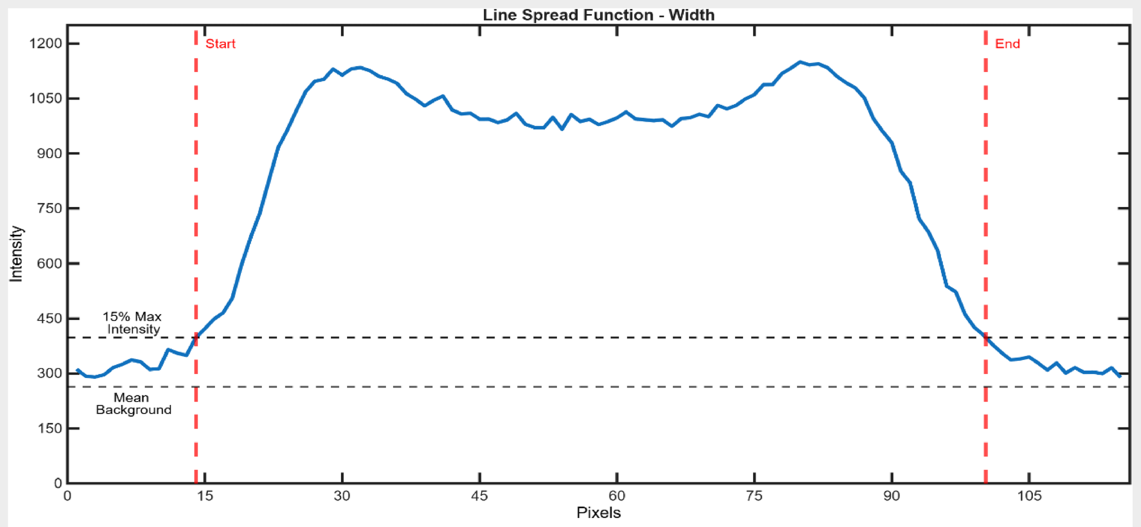

Fig. 6. LSF extracted from Fig. 5(c) after left-right projection. Data were rescaled, thus not directly comparable to raw data Fig. 4(a).

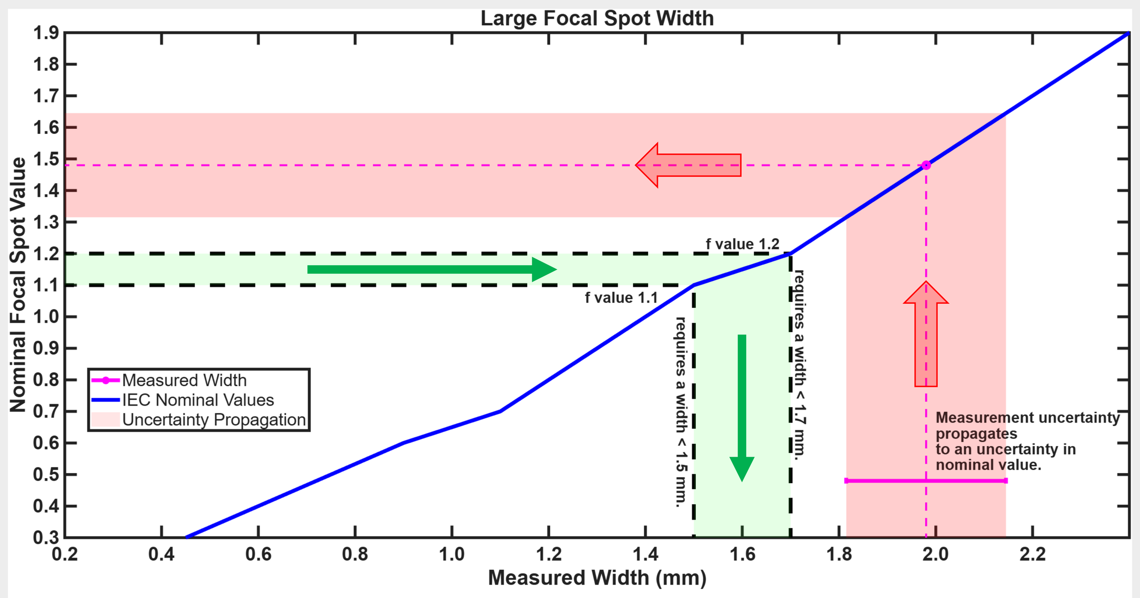

Fig. 7. Graphical generation of uncertainty in IEC nominal value f, evaluated for the width dimension.

Uncertainty in measured focal spot dimension was translated to **uncertainty in IEC nominal value *f*** graphically, as in Fig. 7. For this example f from the measured width is between 1.4 and 1.7, with most likely value 1.5. For height (not shown) the most likely value is 1.4, range 1.2 to 1.6.

For future work, a **camera structure** has been designed (Fig. 8) for **precise alignment of detector, focal spot, pinhole**, and an **optional scale object** with which E can be inferred when the tube is inaccessible for measurement. Its skeleton is **three stackable aluminum box frames**, whose combinations will provide 7 possible d_{SP} values.

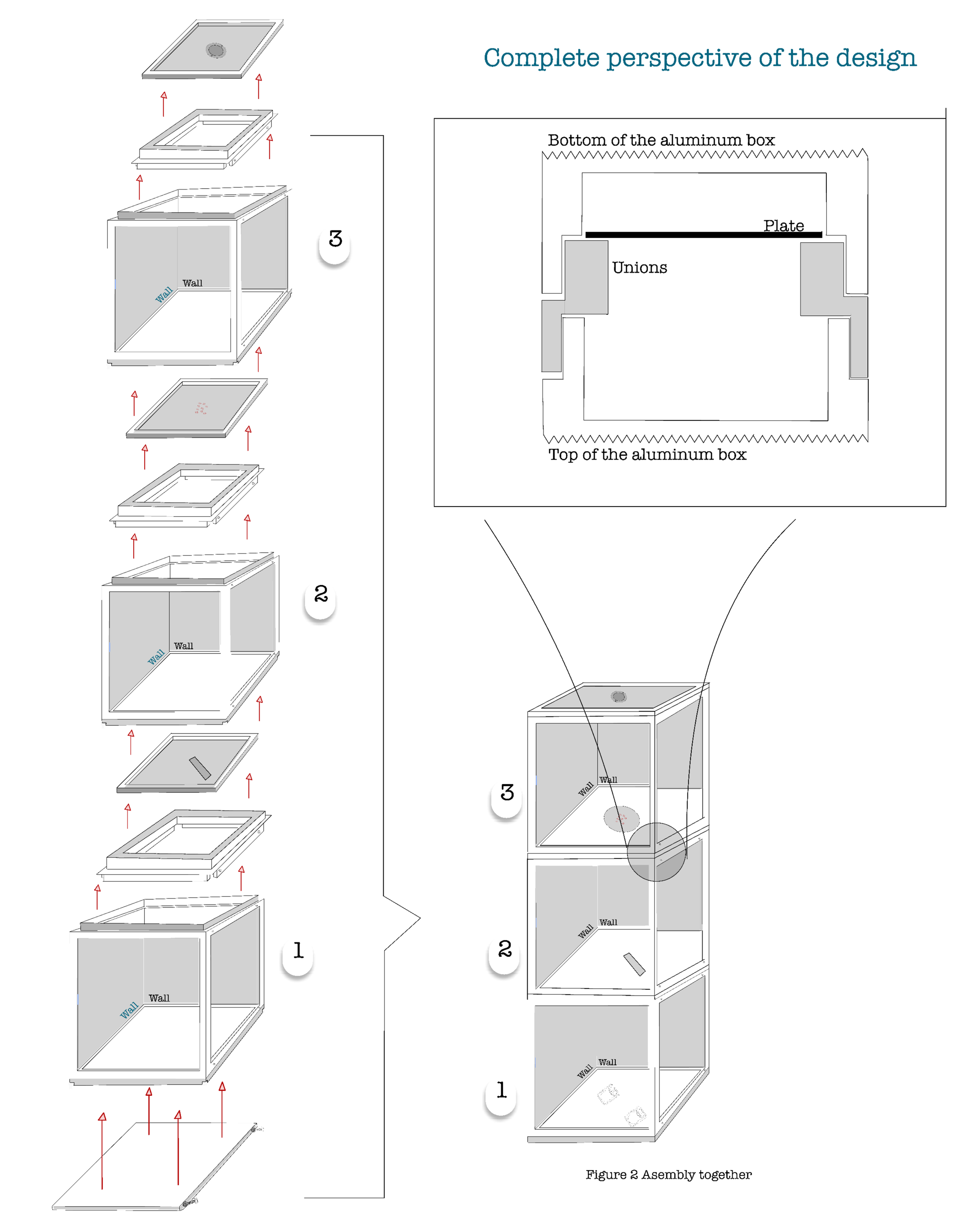

Fig. 8. Modular design for mechanical alignment.

DISCUSSION

Referring to the IEC requirements, for this poster's example assessment of a source with serial plate *f* = 1.2,
(i) our measured dimensions were 1.98 mm x 2.74 mm, both of which exceed the IEC maxima,
(ii) typical signal was > 100 above background,
(iii) SNR in our studies at most 16, more typically under 10.
This method **finds focal spot size and its uncertainty**. In addition the **uncertainty in *f* is obtained** by propagating uncertainties in E, in pinhole and detector blur, and in image measurements. While **due to image faintness our use of pinhole radiography does not meet IEC requirement (iii)**, we obtain **direct visualization of PSF_{source}** which is **more informative** than simply the LSF or just f especially for imaging system design and optimization.

ACKNOWLEDGEMENTS

Thanks to Jack Rubio and Prof. Tong Xu for assistance. Thanks to NSERC (Natural Sciences & Engineering Research Council) for a Discovery Grant (P. Johns), Mitacs for a Global Research Internship (A. Ramos Moreno), and Hamamatsu Corp. for providing the S11684-12 detector at no cost for research studies.